SAND2006-6432C

Experimental Measurements of Thermal Accommodation Coefficients for Microscale Gas-Phase Heat Transfer

W. M. Trott[1], D. J. Rader[2], J. N. Castañeda[3], J. R. Torczynski[4], and M. A. Gallis[5]
Engineering Sciences Center, Albuquerque, New Mexico 87185-0834 USA

An experimental apparatus is described that measures gas-surface thermal accommodation coefficients from the pressure dependence of the conductive heat flux between parallel plates separated by a gas-filled gap. Heat flux between the plates is inferred from measurements of temperature drop between the plate surface and an adjacent temperature-controlled water bath. Thermal accommodation coefficients are determined from the pressure dependence of the measured heat flux at a fixed plate separation. The apparatus is designed to be flexible enough to conduct tests with a variety of gases (monatomic, diatomic, polyatomic, mixtures) in contact with interchangeable, well-characterized surfaces of different materials (e.g., metals, ceramics, semiconductors) and surface finishes (e.g., smooth, rough). Initial experiments are reported for three gases (helium, argon and nitrogen) in contact with pairs of 304 stainless steel plates prepared with one of two finishes: standard machined (lathed) or polished. For argon, the measured accommodation for machined or polished plates are indistinguishable within experimental uncertainty. The accommodation coefficients for machined or polished plates are also indistinguishable for nitrogen. Thus, the accommodation coefficients of 304 stainless steel with nitrogen and argon are estimated to be 0.80±0.02 and 0.87±0.02, respectively, independent of the surface roughness within the range likely to be encountered in engineering practice. The accommodation coefficients of helium are much lower and show a slight variation with 304 stainless steel surface roughness: 0.36±0.02 for the standard machine finish and 0.40±0.02 for the polished finish. Tests are in preparation using materials and finishes of interest to microscale devices, including silicon, polysilicon, semiconductors, and gold.

Nomenclature

$\overline{c}$	=	gas mean molecular speed, $\left(8k_BT/\pi m\right)^{1/2}$
E_{in}	=	incident energy flux
E_{re}	=	reflected energy flux
E_w	=	wall-equilibrium reflected energy flux
k_B	=	Boltzmann constant, 1.380658×10^{-23} J/K
K	=	gas thermal conductivity
L	=	plate separation
m	=	gas molecular mass
P	=	gas pressure
q	=	heat flux magnitude
q_C	=	continuum heat flux
q_{FM}	=	free molecular heat flux
T	=	gas temperature
T_c	=	temperature of cold wall

[1] Technical Staff, Thermal Fluid Experimental Sciences Department, MS 0834, AIAA Non-Member.
[2] Manager, Microscale Sciences and Technology Department, MS 0826, AIAA Non-Member.
[3] Technologist, Thermal Fluid Experimental Sciences Department, MS 0834, AIAA Non-Member.
[4] Technical Staff, Microscale Sciences and Technology Department, MS 0826, AIAA Non-Member.
[5] Technical Staff, Microscale Sciences and Technology Department, MS 0826, AIAA Non-Member.

T_h = temperature of hot wall
ΔT = temperature drop between embedded center and immersed thermistors
ΔT_{rad} = temperature drop contribution from radiation
ΔT_{gas} = temperature drop contribution from gas conduction
z = Cartesian coordinate normal to plates

Greek Variables

α = thermal accommodation coefficient
α_c = cold-wall thermal accommodation coefficient
α_h = hot-wall thermal accommodation coefficient
ζ = number of internal degrees of freedom
λ = gas molecular mean free path
μ = gas viscosity
ρ = gas mass density

I. Introduction

Heat transfer to surfaces immersed in noncontinuum (transitional or rarefied) gas flow continues to be an active area of research. Gases exhibit noncontinuum effects when the characteristic length scale of the system becomes comparable to the molecular mean free path, l, defined as the average distance traveled by a molecule between collisions. As the definition of mean free path is somewhat arbitrary, a number of definitions persist in the literature; the definition of mean free path given by Springer[1] is used here:

$$\lambda = \frac{2\mu}{\rho \bar{c}}, \tag{1}$$

where μ and ρ are the gas viscosity and mass density, and $\bar{c}$ is the mean molecular speed. Noncontinuum effects become important as system length scales become microscopically small or as gas pressures become low. The rise of noncontinuum behavior with decreasing pressure results from the inverse dependence of the mean free path on gas mass density, as given in Equation (1).

Applications with microscopic length scales have grown in importance since the advent of Micro Electro Mechanical Systems (MEMS), which are currently manufactured with micron-scale geometric features. Microsystems are usually operated in air at ambient pressure and temperatures, for which the mean free path is ~0.065 μm.[2] Since the mean free path is not negligibly small compared to the geometric length scales, the conduction of heat across small gas channels exhibits noncontinuum features. One example of a MEMS system in which noncontinuum heat flux must be considered is the microscale thermal actuator shown in Figure 1.[3] Microscale thermal actuators are long beams separated from the substrate by a thin gas-filled gap. When electrical current is passed along the beam, Joule heating produces a temperature rise, causing a proportional length increase which is used to translate a shuttle. The temperature rise is determined by a balance between Joule heating and heat loss to the substrate. This heat loss occurs by conduction along the beam to the anchor points and across the gas-filled gap (radiation is usually small). Microscale gas-phase heat conduction in this device is noncontinuum because the ~1-μm gaps are comparable to the mean free path at atmospheric pressure.[3]

Consequently, thermal management analyses in microsystems must include noncontinuum capabilities. A priori prediction of noncontinuum, gas-phase heat flux requires a detailed description of the gas-surface interaction. Unfortunately, reliable gas-surface interaction mechanisms are lacking for the materials and finishes encountered in the rapidly evolving microsystem arena. A few studies in this area are beginning to appear. Yang and Bennett[4] report molecular-beam measurements of thermal accommodation coefficients for nitrogen reflecting from single-crystal silicon and polyimide surfaces although the high temperatures (1650 K) and low pressures (12 Torr) of these experiments differ substantially from typical microsystem operating conditions (air at ambient conditions). Ideally, a reliable, experimentally-validated database of gas-

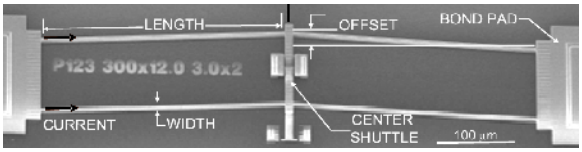

Figure 1. Microscale thermal actuator.

surface interaction models is needed for the wide range of gas-surface combinations that are likely to be encountered in modern microsystem applications.

A major step toward meeting this need has been the development of an experimental apparatus and supporting diagnostics that can provide measurements of gas-surface thermal accommodation coefficients.[5,6] Initial experiments using this apparatus are reported here for three gases (helium, argon and nitrogen) in contact with pairs of 304 stainless steel plates prepared with one of two finishes. One is a standard machined (by lathe) finish that provides a macroscopically rough surface, while the second is a mirror-polished finish that provides a relatively smooth surface. Future plans include tests with materials and finishes of greater interest to microsystems, such as silicon, polysilicon, and gold.

II. Gas-Surface Interactions

Momentum and heat transfer to surfaces immersed in noncontinuum gas flows continues to be the subject of many studies since Maxwell's pioneering work over 100 years ago.[7] To predict momentum and heat fluxes, it is essential to know the net balance of energy and momentum carried by molecules impinging on and reflecting from a surface. Despite considerable efforts to understand this process, detailed gas-surface interaction mechanisms are still lacking.[8]

In the absence of detailed gas-surface interaction models, theoretical predictions for stress and heat transfer usually can be brought into agreement with experimental observations by using empirical parameters called accommodation coefficients. The most widely used parameter for heat transfer is the thermal accommodation coefficient, α , which is defined by

$$\alpha = \frac{E_{in} - E_{re}}{E_{in} - E_{w}}, \tag{2}$$

where E_{in} is the incident energy flux, E_{re} is the reflected energy flux, and E_{w} is the energy flux that would be achieved if the reflected molecules were emitted in thermal equilibrium at the surface temperature.[1,9] The thermal accommodation coefficient varies between unity (complete accommodation, diffuse reflection) and zero (adiabatic, specular reflection). The simple partition of gas-surface collisions into a diffuse, fully accommodated fraction and a specular fraction is often referred to as the Maxwell wall model, a convention which is followed in this work. Note that Equation (2) represents an average over a finite area of surface and a very large number of gas-surface collisions. Also, no attempt is made in Equation (2) to distinguish among the possibly different accommodations for the various molecular degrees of freedom. Thus, the net flux of translational energy is lumped together with that of rotational and vibrational energy, if present. A recent experimental study reports that the thermal accommodation coefficients for translational energy are slightly higher than those for internal energy for a few selected gases in contact with a tungsten wire.[10] Studies that separate contributions to the accommodation coefficient of the different energy modes for other gas-surface combinations are not common.[11]

Previous experimental studies have measured the thermal accommodation coefficient in a variety of geometries and over a wide range of gas-surface combinations.[1,11] The data show that accommodation depends on the composition and temperature of the gas and surface, on gas pressure, and on the state of the surface (roughness, contaminant adsorption, gas adsorption). Experimental values reported for the thermal accommodation coefficient range from 0.01 to nearly unity, depending on the gas-surface combination and the level of contaminants adsorbed on the surface. The smaller values tend to be observed for light gases striking surfaces composed of higher-atomic-weight molecules (e.g., helium striking a clean tungsten surface[10]); near-unity values tend to be observed for heavy gases striking lower- or similar-molecular-weight or contaminated surfaces (e.g., xenon on platinum[11]). Qualitative theoretical arguments predict that thermal accommodation tends to increase with increasing gas molecular weight and with roughness for a given surface. A key limitation of the existing data base, however, is the lack of accommodation data for surfaces encountered in present-day microsystems.

III. Parallel-Plate Heat Transfer

In this study, the gas-surface thermal accommodation coefficient is inferred from experimental measurements of the pressure dependence of heat flux across a gas-filled gap between two parallel disks of unequal temperature. This finite geometry is closely related to the Fourier problem, which is defined as a quiescent gas occupying the region

between two infinite, parallel plates of unequal temperature. A schematic diagram of this geometry is shown in Figure 2. The two plates are separated by a gap, L, and the coordinate system is defined such that $z = 0$ corresponds to the surface of the bottom plate. The temperature of the top plate, T_h, is assumed (without loss of generality) to be higher than that of the lower plate, T_c. In the present experiments, these two temperatures do not differ by much, so the assumption $T_h - T_c << T_c$ is typically satisfied. Because of the imposed temperature difference, heat is conducted through the gas from the hot plate to the cold plate. Since the gas is quiescent (no mass flow), the gas-phase heat transfer between the plates is dominated by conduction and convection is neglected. Radiation is not treated theoretically in this section but is considered in the experimental analysis below.

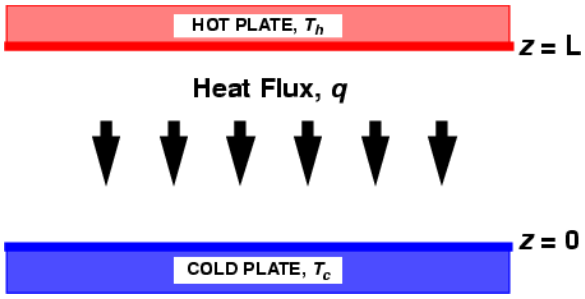

Figure 2. Schematic diagram of Fourier geometry.

A Maxwell gas-surface interaction model[7] is considered, for which a fraction, α, of molecules is reflected diffusely with complete thermal accommodation, while the remaining fraction of molecules, $1-\alpha$, is reflected specularly. Molecules undergoing a diffuse reflection possess a half-range Maxwellian molecular velocity distribution at the wall temperature. For a specular reflection, the tangential velocity of a molecule is left unchanged while the normal velocity changes sign but not magnitude. A purely diffuse surface would be characterized by $\alpha = 1$, a purely specular surface would have $\alpha = 0$, while in the general case the surface accommodation coefficient would lie somewhere in between, $0 \le \alpha \le 1$. In general, each wall would be expected to be characterized by a separate accommodation coefficient. Thus, α_h would be associated with the hot wall, and α_c with the cold wall. In practice, however, the experiments presented here are performed with the careful intent to maintain the materials and surface finishes of the two plates as similar as possible. In this case, the assumption is made that there is only one accommodation coefficient, $\alpha = \alpha_h = \alpha_c$.

In the free molecular limit ($\lambda >> L$), molecules travel back and forth between the plates without colliding with each other. In this case the heat transfer between the plates can be described from a molecular point of view in which the space between the walls is characterized by two streams of non-collisional molecules: higher-energy molecules stream downward from the hot plate and lower-energy molecules stream upward from the cold plate. For a stationary gas with ζ internal degrees of freedom, Bird[12] has shown that the total heat flux to a surface is increased by a factor of $(1+\zeta/4)$ compared to the translational heat flux. Thus, the monatomic-gas result for the free molecular heat flux, q_{FM}, can be extended to a polyatomic gas for the case of small temperature differences ($T_h - T_c << T_c$) and equal wall accommodation coefficients:

$$q_{FM} = -\frac{1}{2}\left(\frac{P\bar{c}}{T}\right)\left(\frac{\alpha}{2-\alpha}\right)\left(1+\frac{\zeta}{4}\right)(T_h - T_c), \tag{3}$$

where $T = T_h^{1/2} T_c^{1/2}$. The free molecular heat flux is directly proportional to the gas pressure, P; in the limit of vanishing pressure, the heat flux approaches zero, as it must in a vacuum.

In the continuum limit ($\lambda << L$), heat flux is described by Fourier's heat-conduction law. In this case, the continuum heat flux, q_C, is given by

$$q_C = -K(T)\frac{dT}{dz}, \tag{4}$$

where K is the gas thermal conductivity, which depends on temperature. Equation (4) applies equally well for any gas (i.e., monatomic, diatomic) if the appropriate value of K is used. The one-dimensional nature of the Fourier geometry requires that the heat flux be constant across the domain (independent of z). Note that the thermal conductivity is independent of pressure; hence, the heat flux is also independent of pressure as long as the flow lies in the continuum regime. For small temperature variations, the thermal conductivity can be assumed to be constant, and Equation (4) can be integrated to obtain:

$$q_C = -K\left(\frac{T_h - T_c}{L}\right). \tag{5}$$

The prediction of the heat flux in the transition regime that lies between the free molecular and continuum limits is challenging, ultimately requiring a complete solution of the Boltzmann equation. Although many theoretical analyses are available in the literature,[1] few result in closed-form expressions for the heat flux. One exception is the analysis of Liu and Lees,[13] who used a four-moment solution of the linearized Boltzmann equation for a monatomic gas to derive an approximate, closed-form expression for the heat flux. Springer[1] extended Liu and Lees' analysis to polyatomic gases and presented the following expression for the heat flux, q, which is intended to apply over the entire pressure range:

$$\frac{q}{q_C} = \frac{1}{1+\dfrac{q_C}{q_{FM}}} = \frac{1}{1+\dfrac{2KT}{L\left(\dfrac{\alpha}{2-\alpha}\right)\left(1+\dfrac{\zeta}{4}\right)\overline{c}P}}, \tag{6}$$

which assumes small temperature differences and equal wall accommodation coefficients. Springer[1] has shown that Equation (6) agrees reasonably well with the limited available experimental data for monatomic and diatomic gases over a wide range of conditions. Independently, Sherman[14] suggested a simple interpolation formula for heat flux that has the same form as Equation (6), except that he allowed the continuum and free molecular heat fluxes to be calculated from their complete (not linearized) expressions. For convenience, Equation (6) is referred to as the "Sherman-Lees" interpolation formula for heat flux.

For analysis of the experimental data to be presented later, it is convenient to rewrite Equation (6) in the following form:

$$\frac{1}{q} = \frac{1}{q_C} + \frac{1}{q_C}\cdot\frac{2KT}{L\left(\dfrac{\alpha}{2-\alpha}\right)\left(1+\dfrac{\zeta}{4}\right)\overline{c}}\cdot\frac{1}{P}. \tag{7}$$

IV. Experimental Setup

This section provides a brief description of the design and operation of the experimental apparatus (shown in Figure 3) that is used in the present study.[5,6] A vacuum test chamber was designed to accommodate all of the control systems and diagnostics needed to provide heat-flux measurements between two parallel, 14.25-cm-diameter plates separated by ~1-cm gas-filled gaps. To provide a high degree of accuracy, state-of-the-art components were selected for controlling system pressure, flow rate, plate alignment, plate temperatures, plate positions, system pressure, and system temperature.

A schematic of the vacuum test chamber design is shown in cross section in Figure 4. The test chamber is a 41-cm-diameter sphere with six 33.66-cm (13.25-in) OD standard conflat flanges mounted in a symmetric pattern (four of the six flanges are shown). The opposing upper and lower flanges were used to mount the upper and lower plate assemblies. An observation window (optical-quality quartz) occupies the flange extending out of the plane in Figure 4, while a cryogenic pump occupies the flange extending into the plane of the figure. Separate chambers are indicated that house an electron gun for gas density

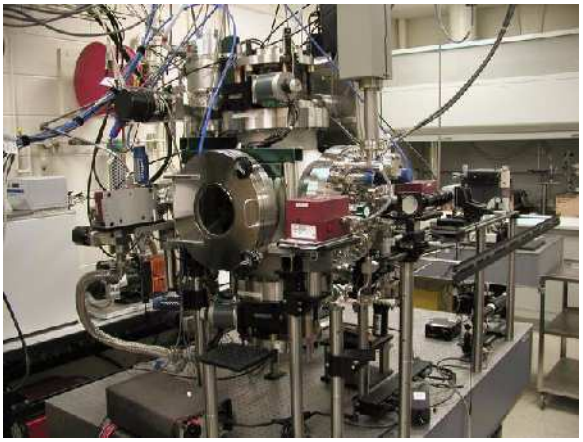

Figure 3. Front view of assembled test apparatus.

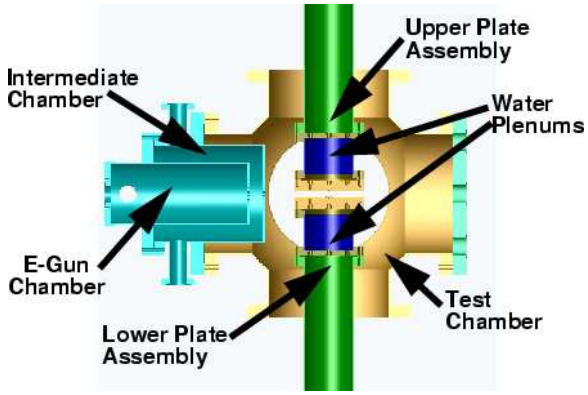

Figure 4. Schematic diagram of vacuum chamber.

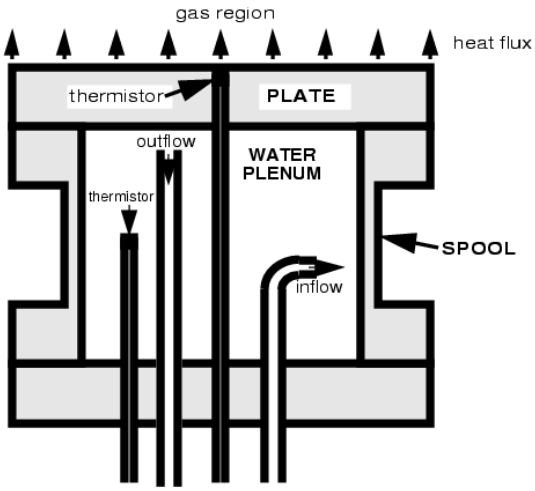

Figure 5. Schematic diagram of "spool" assembly.

measurements using electron beam fluorescence;[5] no measurements with this device are reported here.

Stable control and accurate measurement of gas conditions in the test chamber are essential. Pressure measurements are made using five MKS 690A high-accuracy Baratron pressure transducers (0.05% of full scale). Chamber pressure is actively controlled by comparing the Baratron-measured pressure with an operator-selected pressure set-point; an MKS 244E pressure/flow controller maintains the desired pressure by regulating the flow into the chamber through an automated MKS 245 proportioning control valve. Tests show that the flow controller provides exceptionally stable chamber pressures; for example, the system can maintain a pressure of 30.00±0.01 mTorr over long periods of operation. Thus, the pressure-measurement and flow-regulation subsystems provide extremely accurate and precise control.

Significant care was given to the design of the assemblies which hold the test plates (whose working surfaces are in contact with the gas and determine the gas-surface interface). The plate assemblies were designed to meet several aggressive requirements: 1) maintain a constant temperature across the test plate surface, 2) precisely position each plate independently, 3) maintain parallel alignment between the two plates, 4) provide thermistor access for heat-flux measurements, and 5) allow for ~1-day interchange of plates.

To provide interchangeability, the test plates are based on a commercially-available 6-inch conflat flange that was reduced to a 14.27-cm OD. The experiments reported here use 2.54-cm-thick, 304 stainless steel conflat flanges whose surfaces are finished in different ways (see below). The test plate is secured to a "spool" assembly, which provides direct contact between a 0.62-liter plenum of water and the back side of the test plate (see Figure 5). Two temperature-controlled water baths provide independent control of the temperature of the upper and lower water plenums. Three high-precision Hart Scientific thermistors (stated accuracy 0.01°C) are embedded to within ~1.6 mm of the surface of each test plate: one thermistor is centered, while the other two (not shown in Figure 5) are positioned at a radius of 1.5 inch (3.8 cm). One thermistor is submerged within the water plenum of each spool. The embedded thermistors are used to measure plate temperature and to check for uniformity, while the difference between the centered, embedded thermistor and the submerged, bath thermistor is used to infer heat flux (see below). The thermistors are precise (repeatable) to better than 0.005°C in day-to-day operations. It is this extremely high degree of measurement precision that enables the accurate heat-flux measurements that are described below.

The spool assemblies are mounted to extension columns (see Figure 4) and extensible metal bellows that seal to the top and bottom flanges of the test chamber. The vertical position of each plate assembly is controlled by a separate precision positioner (Thermionics). These positioners can adjust the vertical position of the ~20-kg plate assemblies independently with ~10-micron accuracy. Software is used to control the position of each plate assembly independently or to operate the two positioners in a master/slave mode to maintain a fixed distance between the plates.

Tests are performed on pairs of plates whose surfaces are prepared to be as similar as possible (so that the accommodation coefficients of both surfaces are nearly equal). Two surface finishes have been tested so far, and both are based on a 2.54-cm-thick, 304 stainless steel conflat flange. One pair of plates was prepared with a standard machined (rough) finish with an RMS roughness of ~2 μm, while a second pair of plates was polished to a mirror

(smooth) finish characterized by an RMS roughness of ~20 nm—a hundredfold reduction in surface roughness. Measurements of the thermal accommodation coefficient of these two pairs of plates are presented below.

V. Heat Flux Measurements

Temperature-difference measurements are used to infer the axial heat flux between the two test plates.[5,6] For this purpose, the temperature difference of interest is between a central thermistor embedded just beneath the test-plate working surface and another immersed in the adjacent water plenum (see Figure 5). This is a challenging measurement strategy, as the heat flux through a low-pressure gas is known to be extremely small. The measurement is further complicated by the fact that the thermal conductivities of solids and liquids are very large compared to those of gases. Consequently, the temperature differences across the water plenum and stainless steel plate are found to be extremely small but measurable given the high precision of the Hart thermistors.[5,6]

As an example, Figure 6 shows measured temperature (top) and temperature-difference (bottom) histories for nitrogen in contact with the machined 304 stainless steel plates. The test was conducted with an inter-plate gap of 5 mm and bath temperatures of 15°C and 35°C (approximately symmetric about room temperature). Thermistor readings were recorded with the chamber held near vacuum (left side of the plots) and at pressures between 1 and 6700 mTorr (series of steps moving to the right side of the plots). Histories are shown in Figure 6 only for the embedded and the immersed thermistors of the hot plate.

The determination of heat flux based on temperature measurements assumes that the temperature difference between the embedded and immersed thermistors is linearly proportional to the heat flux. Taking advantage of symmetry, the difference between the temperatures of the central embedded thermistor, T_{cen}, and the immersed thermistor, T_{imm}, is considered. Temperature-difference histories for the data are presented in Figure 6 (bottom), where the magnitude of the differences is $|T_{cen} - T_{imm}|$. One immediate observation is that the pressure steps are now better defined. This improvement is a result of the difference operation, which removes intermediate- and long-term drifts in the liquid-plenum temperature. Although these drifts are reasonably small (~0.05°C over 5 hours), they act to conceal the true trend of the temperature differences. For constant conditions (e.g., fixed pressure, gap, plate temperatures), averaging the temperature difference over time (30-60 minutes) significantly improves the signal-to-noise ratio of the measurements. Using time averaging, the current apparatus can resolve temperature-difference steps as small as ~0.001°C. For example, when pressure is changed from 1 to 3 mTorr, the measured temperature difference increases by 0.009°C, about one order of magnitude larger than the minimum resolution (see Figure 6). Clearly, very small changes in heat flux are resolved with the current system.

The next step in determining gas-phase conduction is to subtract parasitic heat losses that are always present in the system but can be observed in isolation at vacuum. In the absence of gas, any heat flux through the test plates must result from either radiation or solid conduction. For the present apparatus, it is believed that the majority of the parasitic loss results from radiation. Thus, in the following discussion, parasitic losses observed under vacuum are

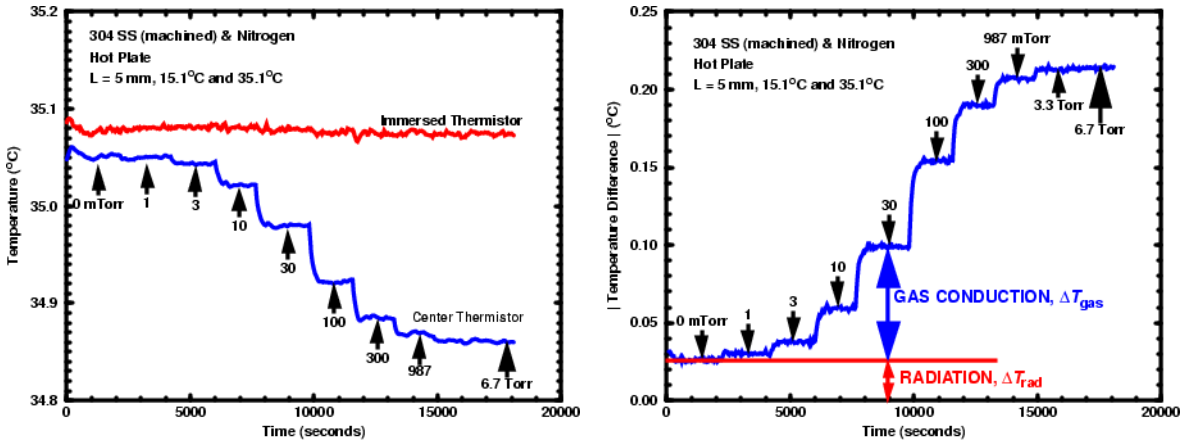

Figure 6. Temperature (left) and temperature-difference (right) histories for the hot plate (nitrogen, machined 304 stainless steel, 5-mm gap).

attributed to radiation. Radiation heat losses are clearly evident in Figure 6 for the 0-mTorr cases; this heat-loss contribution is labeled "RADIATION" in the figure and gives a temperature difference of $\Delta T_{rad} = 0.026°\text{C}$. The temperature-difference contribution from gas-phase conduction, ΔT_{gas}, is determined by subtracting the temperature difference observed under vacuum, ΔT_{rad}, from the total temperature difference:

$$\Delta T_{gas} = \Delta T - \Delta T_{rad} . \tag{8}$$

Although the radiation contribution is much smaller than gas-phase conduction at higher pressures, at pressures below a few mTorr radiation dominates.

The final step in determining heat flux from temperature-difference measurements is to establish a calibration point. One possibility is suggested by the high-pressure data of Figure 6, which show that the measured temperature difference plateaus for pressures above ~5 Torr. The explanation for this behavior is that the continuum limit has been achieved, for which the gas-phase heat flux becomes independent of pressure. The continuum heat flux, q_C, can be calculated using Equation (5), the plate separation, and gas properties. Heat fluxes at arbitrary pressures are determined by the scaling:

$$\frac{q}{q_C} = \frac{\Delta T_{gas}}{\Delta T_C} , \tag{9}$$

where

$$\Delta T_C = \lim_{P\to\infty}\left(\Delta T_{gas}\right) = \lim_{P\to\infty}\left(\Delta T - \Delta T_{rad}\right) . \tag{10}$$

Under the assumption that ΔT_{gas} is proportional to heat flux, q, it is possible to rewrite Equation (7) in a form that is convenient for data analysis:

$$\frac{1}{\Delta T_{gas}} = \frac{1}{\Delta T_C} + \frac{1}{\Delta T_C}\cdot\frac{2KT}{L\left(\frac{\alpha}{2-\alpha}\right)\left(1+\frac{\zeta}{4}\right)\bar{c}}\cdot\frac{1}{P} . \tag{11}$$

Equation (11) is not rigorous, being based on two assumptions: 1) that the Sherman-Lees interpolation formula correctly describes the pressure-dependence of gas heat flux, and 2) that the measured temperature differences are linearly related to the heat flux. Nevertheless, Equation (11) is proposed as a means of correlating the experimental measurements of ΔT_{gas} as a function of pressure. The form of Equation (11) suggests that a plot of $1/\Delta T_{gas}$ against inverse pressure, $1/P$, should be linear. A graphical interpretation of such a plot is that the y-axis intercept equals the reciprocal of the continuum-limit temperature difference, ΔT_C, and the slope is a function of known quantities and the accommodation coefficient. Thus, regression of data such as are shown in Figure 6 can be used to determine a best-fit value for the slope from which the accommodation coefficient is extracted.[5,6]

VI. Experimental Results

A. Machined (Rough) Plate Results

Measurements of ΔT_{gas} as a function of pressure were made with the pair of machined (rough) 304 stainless steel plates (RMS roughness of ~2 μm) in contact with helium, argon, and nitrogen.[5,6] For each gas-plate combination, several tests were performed using different combinations of plate separation and hot and cold plate temperatures. The data have been analyzed in the manner described above and plotted in the form suggested by Equation (11). For example, the raw data for nitrogen shown in Figure 6 (5-mm gap, $T_c = 15.1°\text{C}$ and $T_h = 35.1°\text{C}$) are replotted in Figure 7 for the near-continuum pressure range $30 < P < 6700$ mTorr ($4.0 < P < 893.3$ Pa). Data for both the cold and hot plates are shown. The linear nature of the data when plotted in this fashion is evident. Linear regressions to the data from each plate give correlation coefficients near unity, $r^2 = 0.99999$. The reciprocal of the regression intercepts give continuum-limit temperature differences of $\Delta T_C = 0.2152$ and $0.1895°\text{C}$ for the

cold and hot plates, respectively. Inspection of the hot-plate temperature histories plotted in Figure 6 reveals that the 6.7-Torr measurement has reached 99% of the continuum limit.

The regression slopes can be used to determine the thermal accommodation coefficient according to Equation (11). The resulting values for the cold and hot plate, $\alpha = 0.808$ and 0.795, respectively, are in excellent agreement. This is a satisfying result, as the heat flux between the two plates must be exactly equal in the ideal one-dimensional situation when parasitic heat losses and nonlinearities are neglected. The results reported here are consistent with a Maxwell wall model in which 80% of nitrogen molecules undergo a diffuse, thermally-accommodated reflection, while the remainder undergo a specular reflection. Moreover, the good agreement between data and regression in Figure 7 suggests that the Sherman-Lees interpolation function works well in the near-continuum regime.

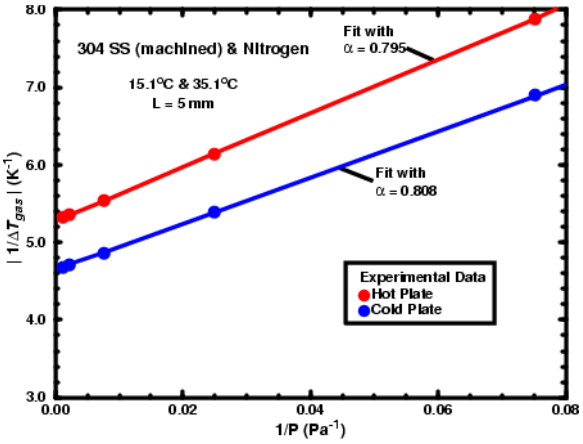

Figure 7. Plot of inverse ΔT_{gas} vs. inverse pressure in the near-continuum regime (nitrogen, $T_c = 15.1°C$, $T_h = 35.1°C$, machined 304 stainless steel, 5-mm gap).

Similar tests were made with the machined plates with argon and helium. The conditions used for the argon tests were: 10-mm gap, $T_c = 5.2°C$ and $T_h = 45.0°C$. The conditions used for the helium tests are: 10-mm gap, $T_c = 20.2°C$ and $T_h = 30.1°C$. The data from these two tests are analyzed in the manner described in the pressure ranges $50 < P < 10000$ mTorr ($6.7 < P < 1333.2$ Pa) for argon and $200 < P < 10000$ mTorr ($26.7 < P < 1333.2$ Pa) for helium. As with nitrogen, good linear fits were obtained with correlation coefficients near unity. The accommodation coefficients calculated for argon for the cold and hot plates, $\alpha = 0.875$ and 0.866, respectively, are in good agreement. The accommodation coefficients calculated for helium for the cold and hot plates, $\alpha = 0.363$ and 0.360, respectively, are also in good agreement.

Based on these and additional tests, the best-estimate accommodation coefficients for helium, nitrogen, and argon in contact with machined (rough) 304 stainless steel is determined to be $\alpha = 0.36$, 0.80, and 0.87, respectively, with an estimated uncertainty of ±0.02 for each value. As suggested by qualitative physical arguments, the accommodation coefficient increases with increasing gas molecular weight. These results are summarized in Table 1.

B. Polished (Smooth) Plate Results

Measurements of ΔT_{gas} as a function of pressure were also made with the pair of polished (smooth) 304 stainless steel plates (RMS roughness ~20 nm) in contact with helium, argon, and nitrogen.[6] The data were analyzed in the same manner as above: the inverse temperature difference was plotted against inverse pressure and the thermal accommodation coefficient was determined from the slope of the best-fit line. Cold-plate data for the polished plates with nitrogen are shown Figure 8; cold-plate data for the machined plates with nitrogen are also shown for comparison. The machined and polished curves are substantially parallel, which implies that the accommodation coefficients are similar. Similar agreement was observed for the polished and machined plates in contact with argon. The best estimates of the accommodation coefficients for argon and nitrogen in contact with the polished plates (taken as the average of the hot- and cold-plate values) are $\alpha = 0.87$ and 0.80, respectively, with an experimental uncertainty of ±0.02. Compared with the above results, the accommodation coefficients for the machined- and polished-plate agree to within experimental uncertainty for both gases. This result is unexpected considering the factor of ~100 difference in surface roughness between the two surfaces.

Table 1. Summary of measured gas accommodation coefficients with 304 stainless steel.

Gas	Machined	Polished
Helium	0.36±0.02	0.40±0.02
Nitrogen	0.80±0.02	0.80±0.02
Argon	0.87±0.02	0.87±0.02

Cold-plate data for helium in contact with the machined and polished plates are shown in Figure 9. The helium results are qualitatively different from the argon and nitrogen data in that the slopes for the two helium experiments are clearly distinguishable,

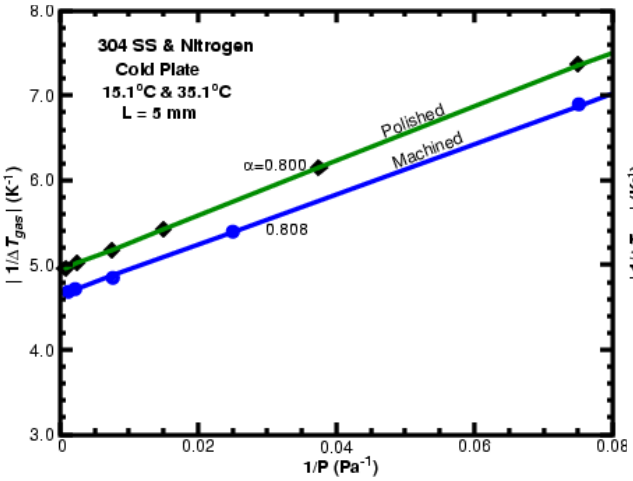

Figure 8. Plot of inverse ΔT_{gas} vs. inverse pressure for machined and polished 304 stainless steel (nitrogen, T_c = 15.1°C, T_h = 35.1°C, 5-mm gap).

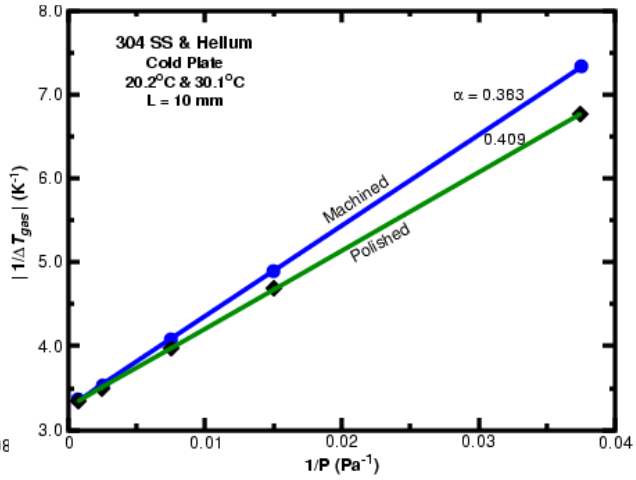

Figure 9. Plot of inverse ΔT_{gas} vs. inverse pressure for machined and polished 304 stainless steel (helium, T_c = 15.1°C, T_h = 35.1°C, 10-mm gap).

implying distinct accommodation coefficients for the two different finishes. Calculation of the best-estimate accommodation coefficient from the average of the values for the hot and cold polished plates gives $\alpha = 0.40 \pm 0.02$. Comparing to the machined-plate results, it appears that there is a small decrease in accommodation with increasing surface roughness for helium and 304 stainless steel although the observed difference is only slightly larger than experimental uncertainties. Suggested values for the accommodation coefficient for helium and 304 stainless steel would be $\alpha = 0.36$ and $\alpha = 0.40$, respectively, for the machined and polished finishes.

VII. Discussion

The present work suggests that macroscopic surface roughness plays only a minor role in determining the thermal accommodation coefficient of 304 stainless steel in contact with helium, argon, and nitrogen. For argon and nitrogen, the machined- and polished-plate accommodation coefficients are indistinguishable, agreeing within experimental uncertainty despite the factor of ~100 difference in RMS surface roughness between the two finishes. Given that these two finishes essentially span the range of surface roughness that can be obtained using conventional machining processes with 304 stainless steel, the preliminary conclusion drawn here is that thermal accommodation coefficients for argon and nitrogen combined with 304 stainless steel are 0.87 and 0.80, respectively, independent of surface roughness. These new accommodation values are in fair agreement with the previously reported values for steel-argon and steel-nitrogen systems of 1.0 and 0.9, respectively.[11] Both the current and the literature values exhibit the same trend with α for argon being ~10% larger than that for nitrogen. The overall agreement is satisfactory considering that the steel alloy and surface finish were not specified.[11]

Surface roughness was found to have a small but distinguishable effect on the accommodation of helium with 304 stainless steel, with values of $\alpha = 0.40$ for the polished finish and $\alpha = 0.36$ for the machined finish. A decrease in accommodation with increasing roughness is not generally expected, as general theoretical arguments would support the opposite. The observed decrease of α with increasing surface roughness is barely larger than the experimental uncertainty and additional studies are needed to verify if this trend can be substantiated. The accommodation values reported here are in good agreement with a previously reported value for a steel-helium system, $\alpha = 0.393$.[11]

VIII. Conclusions

A priori prediction of noncontinuum, gas-phase heat flux in microsystems requires a detailed description of the gas-surface interaction. Because of the physical complexity of the problem, the most effective approach to providing such descriptions involves careful experimental investigations. Unfortunately, experimental data are lacking for the materials and finishes encountered in the rapidly evolving microsystem arena. This study reports on the

development of an experimental apparatus and supporting diagnostics that can provide precise measurements of gas-surface thermal accommodation coefficients, including materials of interest in MEMS applications.

As a demonstration of this new capability, this study reports thermal accommodation measurements of argon, nitrogen, and helium in contact with pairs of 304 stainless steel plates prepared with one of two finishes: standard machined (lathed) or mirror polished. The measured accommodation coefficients for argon and nitrogen in contact with these two finishes are indistinguishable within experimental uncertainty. Thus, the accommodation coefficient of 304 stainless steel with nitrogen and argon is estimated to be 0.80±0.02 and 0.87±0.02, respectively, independent of the surface roughness within the range likely to be encountered in engineering practice. Measurements of the accommodation of helium show a slight variation with 304 stainless steel surface roughness: 0.36±0.02 for the machined finish and 0.40±0.02 for a polished finish. Future plans include tests with materials and finishes of interest to microsystems.

Acknowledgments

This work was performed at Sandia National Laboratories. Sandia is a multiprogram laboratory operated by Sandia Corporation, a Lockheed Martin Company, for the United States Department of Energy's National Nuclear Security Administration under contract DE-AC04-94AL85000.

References

[1]Springer, G. S., "Heat transfer in rarefied gases," *Advances in Heat Transfer*, edited by T. F. Irvine and J. P. Hartnett, Academic Press, New York, NY, 1971, pp. 163-218.

[2]Karniadakis, G. E., and Beskok, A., *Micro Flows: Fundamentals and Simulation*, Springer-Verlag, New York, NY, 2002.

[3]Gallis, M. A., Torczynski, J. R., and Rader, D. J., "A Computational Investigation of Noncontinuum Gas-Phase Heat Transfer between a Heated Microbeam and the Adjacent Ambient Substrate," *Sensors and Actuators A* (to be published).

[4]Yang, H., and Bennett, T. D., "Time of Flight Measurements of Thermal Accommodation Coefficient," *Proceedings of the 34th National Heat Transfer Conference*, NHTC2000-12035, ASME, Washington, DC, 2000.

[5]Rader, D. J., Trott, W. M., Torczynski, J. R., Gallis, M. A., Castañeda, J. N., and Grasser, T. W., "Microscale Rarefied Gas Dynamics and Surface Interactions for EUVL and MEMS Applications," Sandia National Laboratories, Rept. SAND2004-5329, Albuquerque, NM, 2004.

[6]Rader, D. J., Trott, W. M., Torczynski, J. R., Castañeda, J. N., and Grasser, T. W., "Measurements of Thermal Accommodation Coefficients," Sandia National Laboratories, Rept. SAND2005-6084, Albuquerque, NM, 2005.

[7]Maxwell, J. C., *The Scientific Papers of James Clerk Maxwell*, Vol. 2, Cambridge University Press, London, UK, 1890.

[8]Ohwada, T., "Heat Flow and Temperature and Density Distributions in a Rarefied Gas between Parallel Plates with Different Temperatures," *Physics of Fluids*, Vol. 8, 1996, pp. 2153-2160.

[9]Schaaf, S. A., and Chambre, P. L., "Flow of Rarefied Gases," *Fundamentals of Gasdynamics*, Vol. 3, edited by H. W. Emmons, Princeton University Press, Princeton, NJ, 1958, pp. 687-739.

[10]Rebrov, A. K., Morozov, A. A., Plotnikov, M. Yu., Timoshenko, N. I., and Shishkin, A. V., "Using a Thin Wire in a Free-Molecular Flow for Determination of Accommodation Coefficients of Translational and Internal Energy," *Rarefied Gas Dynamics: 23rd International Symposium*, edited by A. D. Ketsdever and E. P. Muntz, AIP Conference Proceedings, Melville, NY, Vol. 663, 2003, pp. 1016-1021.

[11]Saxena, S. C., and Joshi, R. K., *Thermal Accommodation and Adsorption Coefficients of Gases*, Hemisphere Publishing Company, New York, 1989.

[12]Bird, G. A., *Molecular Gas Dynamics and the Direct Simulation of Gas Flows*, Clarendon Press, Oxford, UK, 1994, p. 84.

[13]Liu, C. Y., and Lees, L., "Kinetic Theory Description of Plane Compressible Couette flow," *Rarefied Gas Dynamics*, edited by L. Talbot, Academic Press, New York, NY, 1961, pp. 391-428.

[14]Sherman, F. S., 1963, "A Survey of Experimental Results and Methods for the Transition Regime of Rarefied Gas Dynamics," *Rarefied Gas Dynamics*, Vol. II, edited by J. A. Lauermann, Academic Press, New York, NY, pp. 228-260.